2022 IEEE 5th International Conference on Soft Robotics (RoboSoft)
April 4-8, 2022, Edinburgh, UK

An Electro-pneumatic Shape Morphing Rolling Robot with Variable Locomotion Modes

Chen Liu[1], Oliver Edwards[2], Kaspar Althoefer[1], Ketao Zhang[1], and Hareesh Godaba[2]

***Abstract*— Mobile robots with accurate and fast rolling locomotion capabilities would greatly enhance their adaptability in dynamic environments. Inspired by organisms capable of rolling locomotion, this paper presents a lightweight shape morphable rolling robot which integrates an origami skeleton with muscle-like pneumatic pouches as drivers and electroadhesion (EA) pads as anchors. The origami skeleton of the robot is a hexagonal loop structure composed of polyethylene terephthalate (PET) panels with flexural hinges between them. Pneumatic pouch actuators are embedded between the panels to change the configuration of the skeleton. The flat panels of the origami skeleton house electroadhesion actuators which can adhere to different surfaces with different slopes and materials. Two sequential control schemes are proposed that enable the robot to move forward and backward accurately by controlling the air pressure in the pouches and voltage supplied to the EA pads. Using combined actuation of pneumatic pouches and EA pads, the robot is able to roll on both horizontal and inclined surfaces as well as transit from horizontal to fully vertical surfaces. The robot shows less than 1% error in positioning after one complete forward and backward rolling cycle. Owing to its use of thin sheet materials for skeleton and pouch actuators and EA pads, the robot is lightweight weighing only 25 g. These unique properties of the robot will enable the deployment of such versatile mobile robots to conduct tasks remotely in challenging environments.**

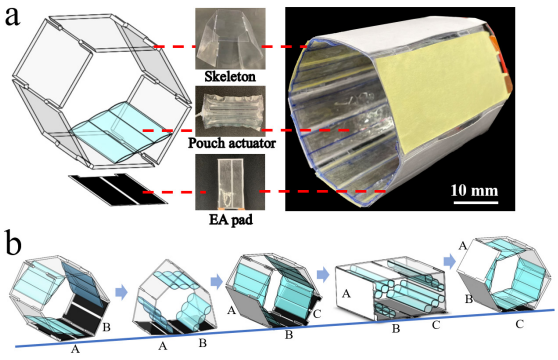

Fig. 1. A shape morphing rolling robot powered by pneumatic pouches and electroadhesion (a) 3D model of the robot showing the skeleton, pouch actuator and an electroadhesion pad. Insets show images of fabricated parts (b) A sequence of images showing the rolling robot execute one step of forward motion in triangle and rectangle locomotion gaits successively.

I. INTRODUCTION

Organisms such as Pleurotya ruralis [1] have evolved capabilities of morphing their body and using rolling as a way of locomotion. Taking these organisms as a source of inspiration, robotic systems imitating rolling as a locomotion strategy have been explored in recent years [2], [3], [4], [5], [6]. Among these developments, rolling robots using soft materials and muscle-like actuation systems display qualities similar to living organisms [7], [8]. They have the ability to manoeuvre through narrow gaps and adjust themselves to work in unconventional environments. While rolling locomotion increases the versatility of robotic movement, it brings several challenges. Rolling robots can encounter slipping making it difficult to control their position precisely. It is also difficult to climb up steep inclines[5], [9]. In addition to these challenges, soft-bodied rolling robots are complex to model and control due to the inherent properties of the soft materials they are made from [10].

To gain the advantages of flexibility and adaptability of soft robots but reduce the complexity, semi-flexible robots with integrated rigid and flexural components have been developed to allow a greater degree of freedom during movement while simplifying model complexity and enabling large payloads [11], [12]. A typical class is origami robots [13], [14], which have programmable deformations as well as a certain degree of rigidity. The use of deformable materials and unconventional kinematic elements in origami robots also requires novel actuation systems. The current driving methods for this type of robots mainly include shape memory alloy (SMA), electric, magnetic and pneumatic actuators. SMA actuators have simple control but the driving speed is relatively low [15], [16]. Dielectric elastomer actuators driven by electric field display high bandwidth and fast response but relatively low output forces [17], [18]. Another class of actuation based on magnetic field utilises magnetic powder embedded in the robots and controls the movement and deformation of the robot via an external magnetic field [19], [20]. The reaction speed is high but the control strategy and programming the magnetic field are difficult tasks. Pneumatic actuation is a relatively mature method, which has the advantage of providing large output force [13], [21], [22]. It is reliable and can be deployed in extreme conditions [23], [24].

It is envisaged that functional foot/anchor allows stable

This work was partially supported by research awards from the Engineering and Physical Sciences Research Council (EPSRC) projects, National Centre for Nuclear Robotics (NCNR) EP/R02572X/1, NCNR Flexifunds Grant, and Queen Mary University of London (QMUL) - China Scholarship Council (CSC) Scholarship. We thank Mr. Yan Wang's assistance with experiments' devices.

[1] C. Liu, K. Athoefer and K. Zhang are with the Centre for Advanced Robotics, Queen Mary University of London, UK chen.liu, k.althoefer, ketao.zhang@qmul.ac.uk

[2] O. Edwards and H. Godaba are with the School of Engineering and Informatics, University of Sussex, UK oe69,h.godaba@sussex.ac.uk

2022 IEEE 5th International Conference on Soft Robotics (RoboSoft) | 978-1-6654-0828-8/22/$31.00 ©2022 IEEE | DOI: 10.1109/ROBOSOFT54090.2022.9762154

movement of rolling robots, especially in complex ground environments, such as ramps and walls [25]. Various foot designs such as bionic suckers have been employed in crawling robots to afford stable movements [26], [27]. However, current rolling robots have relatively few special foot/anchor designs. In recent years, electroadhesion (EA) devices have been used to make robot grippers [28] and feet [18], [29] as well as perching pads to facilitate various functions. Electroadhesion is fast, noise-free, and works on a wide range of materials including both conductive, dielectric, magnetic, and non-magnetic materials [30]. In addition, EA pads can be extremely thin saving space and weight [31], [32] making it conducive for the design of lightweight and imperceptible robot feet for rolling robots.

In this work, we propose a shape morphing electro-pneumatic rolling robot (Fig. 1) that utilizes pneumatically actuated shape-morphing of a flexible structure and combines the controllable adhesion of electroadhesion pads to achieve stable locomotion over horizontal and inclined surfaces as well as being capable of transiting to a vertical surface. The robot is lightweight and flexible. It robot contains six pneumatic muscles and six EA pads. The robot can execute two different locomotion gaits; one related to shape morphing from a hexagon to a triangle and the other to a rectangle. The triangle gait, based on a simple sequential control, enables the robot to execute forward and backward rolling without prior knowledge of the robot's position and orientation using just two pneumatic valves and two high-voltage amplifiers (or switches). The rectangle gait reduces the contraction needed in the pouches to execute rolling and helps the robot climb steeper inclines compared to the triangle gait.

This work makes the following contributions:

1) A novel approach for creating a rolling robot whose body can shape-morph and execute multiple gaits,
2) Integration of a pneumatically actuated morphable structure with EA feet to achieve a light weight robot capable of stable and accurate locomotion, and
3) Simple sequential control technique to steer the robot forward and backward.

In the following sections, we detail the concept of the new shape morphable rolling robot, the design and fabrication of its various components, their characterization and finally demonstration of the rolling motion on horizontal and inclined surfaces as well as transition from horizontal to vertical surface.

II. Concept of the Rolling Robot

The electro-pneumatic shape morphing rolling robot consists of a flexible skeleton with six flat panels connected by six flexure hinges, one pneumatic actuator per flexure hinge, and one electroadhesion pad per panel. The flexible skeleton is realized by cutting a planar PET sheet in a predesigned geometry to realize semi-rigid panels connected by flexure hinges. This 2D sheet is manually converted to a hexagonal skeleton (Fig. 1(a)). A pneumatic pouch actuator attached between two panels deforms when actuated and applies force

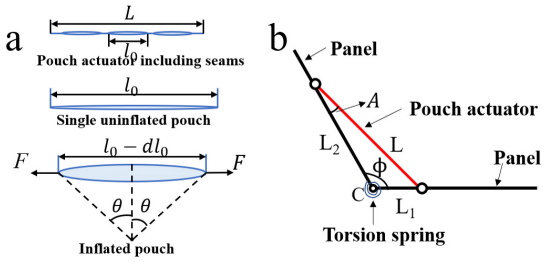

Fig. 2. (a) Free body diagram of a pouch actuator in its uninflated and inflated state. (b) Schematic of a single hinge and panels actuated by a pouch actuator.

to decrease the angle between the panels (Fig. 2(a)). Multiple pouch actuators embedded into the robot skeleton morph its configuration (Fig. 1(b)). The panels house EA pads which generate an electric field when a voltage is applied across the electrodes. This electric field polarises the surface in proximity and makes the EA pad adhere firmly to the surface.

Fig. 3 shows the two locomotion gaits of the rolling robot, they are the triangle locomotion gait (Fig. 3(a)) and the rectangle locomotion gait (Fig. 3(b)). Specific pouch actuators as shown in Fig. 3 are actuated to rotate the hinges to desired angles (60°for the triangle locomotion gait, 90°for the rectangle locomotion gait) to make the robot achieve the triangle and rectangle shapes as shown in (Fig. 3). EA pads on the panels numbered B are now turned on to firmly adhere them to the ground. Setting the pressures in all the pneumatic pouches back to zero, the robot recovers its original hexagonal shape, resulting in advancement by one step. This cycle of pressure and voltage inputs can be repeated to advance the robot forward, while a reversal of the sequence will cause the robot to roll in the opposite direction and roll backward. An even number of panels are needed to achieve such sequential control. With only four panels, the robot needs to execute a fully flat configuration which is challenging. Hence, a hexagonal structure is used for the robot. The actuation sequence and kinematic model of the rolling robot in the two different gaits are shown in the supplementary video.

III. Analytical Modelling

In this section, we present the analytical model of the pouch actuator and that of a flexure hinge actuated by the

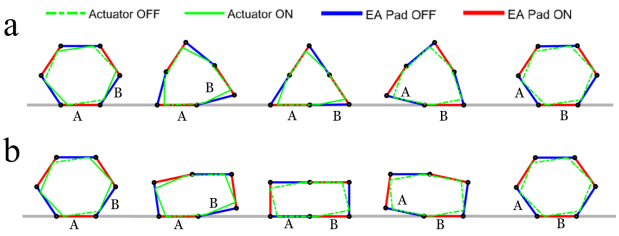

Fig. 3. Illustration showing the sequence of steps of the rolling robot in (a) the triangle locomotion gait and (b) the rectangle locomotion gait.

pouch actuator. We calculate the effect of pouch actuator pressure on the angular deformation of the flexure hinge and analyse the effect of the actuator's attachment location on the panels to find its optimal placement.

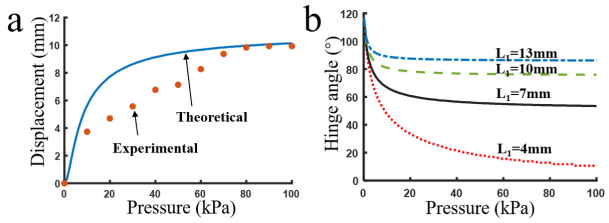

Fig. 4. Modeling of a single hinge driven by pouch actuator. (a) Experimental recording and theoretical fitting of pressure-displacement relation of a single pouch actuator. (b) Pressure vs angular deformation of hinge for different attachment points.

Consider a pouch actuator of width, D and total length, L_0 comprising three individual pouches each of initial length l_0 in their reference configuration when no pressure is applied (Fig. 2(a)). When actuated by a pressure, P the pouches inflate symmetrically about the horizontal midline and contract with each sheet of a pouch form an arc as shown in Fig. 2(a) subtending an angle, θ at the centre of the arc. The current length of each pouch, l is given as a function of θ as follows:

$$l(\theta) = l_0 \cdot \sin(\theta)/\theta \tag{1}$$

However, the pouch actuator has several seams. Considering that segments totalling a length of L_e cannot bulge upon inflation, the current length of the pouch actuator as a function of θ is given by:

$$L(\theta) = L_e + (L_0 - L_e) \cdot \ sin(\theta) \tag{2}$$

When the pouches are inflated, they contract displacing the forces, F applied at the ends of the pouch actuator. From work energy balance, we get: [33]

$$PdV = FdL \tag{3}$$

From geometry of the pouches, volume of each pouch is given as a function of angle θ. The total volume of the pouch is given by the equation below:

$$V(\theta) = \alpha \cdot L_o^2 \cdot D/2 \cdot (\theta - cos\theta \cdot sin\theta/\theta^2) \tag{4}$$

where α is the volume correction factor to account for the reduced volume because of the seams and non-uniform pouch cross-section due to the edges in length direction being sealed. Substituting equation (4) in equation (3), we get:

$$F(\theta) = \alpha \cdot L_0 \cdot D \cdot P \cdot \cos(\theta)/\theta \tag{5}$$

For a given load F and pressure P, the current length of the actuator L can be obtained by solving equations (2) and (5). We first conduct an experiment to identify the pouch parameters L_e and α. We fabricated a pouch actuator of length, 40mm and width, 90mm with three pouch sections. One end of the pouch actuator was clamped to a fixed platform and a mass of 1kg was suspended vertically from the other end. The pressure versus displacement was noted as an average of three trials and is plotted in Fig. 4(a). Equations (2) and (5) were solved to simulate the pressure-displacement relations for different values of L_e and α. The solid line in Fig. 4(a) shows the theoretically fitted curve when L_e=10mm and α=0.65. These identified parameters are used for the rest of the simulation to find optimal attachment points.

Now, let us consider two panels of length L_{panel} and a pouch actuator of length L_0 in its uninflated state. The two panels are connected by a flexure hinge whose resting angle is ϕ_0 and the torsional spring constant is approximated as C. Let the attachment points of the pouch actuator on the two panels be at distances L_1 and L_2 from the hinge. In the current state, the pouch angle (in Fig. 2(a)) is represented by θ, the hinge angle by ϕ, and the length of the pouch actuator by L.

From Fig. 2(b), we can see that the torque, τ in the torsional spring is balanced by the force applied by the pouch actuator on the panels.

$$\tau = F(\theta) \cdot sin(A) = C \cdot (\phi - \phi_0) \tag{6}$$

where A can be calculated from geometry. For any given pressure P, equations (2)-(6) can be solved to find θ and ϕ. Now, we utilise this model to predict the influence of pressure on the hinge angle. Panels of length 40mm are chosen in this project and the torsion stiffness of the flexure hinge, C is experimentally approximated to be $3.27x10^{-4}$ Nm/deg (discussed later in Section V.A.) During the locomotion cycle, the hinge angle changes between 0° and 180°. Therefore, the length of the pouch actuator in the uninflated state should be 40mm to allow the hinge angle to reach 180°. To find the optimal attachment points L_1 and L_2, we calculate pressure versus hinge angle relations for different values of L_1 (shown in Fig. 4(a)). From Fig. 4(b), we observe that, as L_1 decreases, the angular deformation of the hinge increases. However, as the attachment point gets closer to the hinge, the torque generated by the pouch actuator on the panel reduces. So, we optimally select L_1=7mm which allows the hinge angle to reach just under 60 degrees that is needed for the robot to exhibit the triangular gait.

IV. Design and Fabrication

In this section, we introduce the design and procedures for fabricating the morphable skeleton, actuators and assembling them to realize the rolling robot.

A. Morphable structure

A thin planar sheet of polyethylene terephthalate (PET) made into a closed loop 3d structure forms the morphable skeleton of the robot. A 0.35 mm thick PET sheet is taken and cut into the 2D pattern shown in Fig. 5(a) using an electronic cutter (Cricut Maker, Inc. USA.). The 2D pattern consists of six rectangular panels each of width 90 mm and length 40 mm. Consecutive panels are joined by narrow

regions that act as flexure hinges. These narrow regions are manually deformed such that the ends of the first and the last panels become coincident and the flat sheet becomes a 3D structure with a hexagonal cross-section as shown in Fig. 5(c). Another PET panel is used to attach the ends of the first and the sixth panel. The narrow regions connecting the panels are creased during the deformation process and perform as flexural hinges concentrating the deformations due to applied forces on the hinges rather than on the panels.

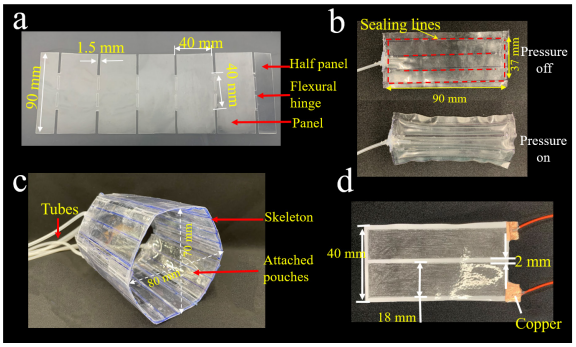

Fig. 5. The manufacturing process of the robot's skeleton. (a) Geometry and dimensions of cut PET sheet. (b) The fabrication process of the pouch actuator. (c) The integration of pouch actuators and the skeleton. (d) Design geometry and fabricated electroadhesion pad.

B. Pneumatic actuator

The morphable skeleton structure is deformed using pneumatic pouch actuators that are integrated with the 3d structure. Pneumatic pouch actuators are made using thermoplastic polyurethane (TPU) sheets of thickness 0.14 mm. A sheet of width 40 mm and length 180 mm is folded into a bilayered film of width 40 mm and length 90 mm. The overlapping edges are firmly sealed using a heat sealer to form an airtight pouch. Further, two more lines are heat-sealed to divide the pouch into three equal interconnected segments. A silicone tube of 1mm diameter is inserted into the air chamber through a tiny hole made on one side (as shown in Fig. 5(b)) to provide a pneumatic inlet. The hole is then sealed using a silicone-based adhesive (Sil-poxy from Smooth-On Inc.). Initially, when no pressure is applied, the pouch actuator is flat with almost no air between the two sheets. When pressure is applied through the pneumatic inlet, air flows into the pouch making it bulge and contract along the shorter edge of the pouch segments. Based on the modelling results shown in Fig. 4, the pouch is attached at a distance of 7 mm and 33 mm from the hinge on the right and left panels respectively.

C. Electroadhesion pad

Electroadhesion allows the robot to attach onto different surfaces enabling it to achieve stable and robust locomotion. As Fig. 5(d) shows, an EA pad consists of two rectangular electrodes of dimensions 17 mm by 86 mm next to each other with a gap of 2 mm between them. The electrodes are realised by shading a 0.1 mm thick paper with 2B pencil

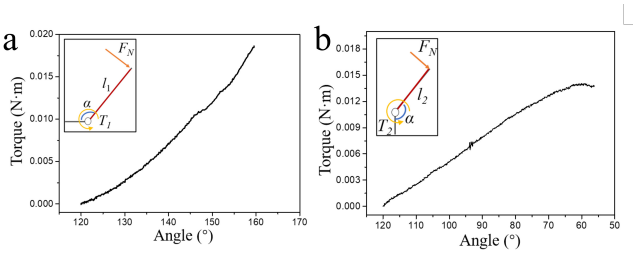

Fig. 6. (a) Torques when the angle of the hinge changing from 120° to 160°. (b)Torques when the angle of the hinge changing from 120° to 60°.

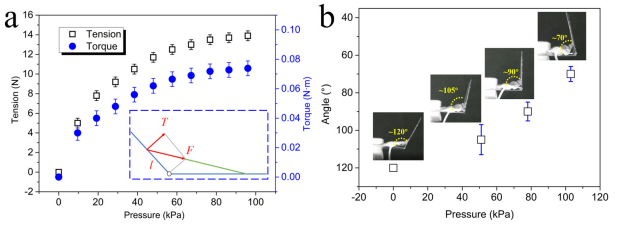

Fig. 7. (a) Tensions and torques to the hinge produced by the pouch actuator at different pressures from 0 kPa to 100 kPa. (b) The driving effect of the pouch actuator on the rotating unit.

lead. This deposits graphite particles on the paper making the shaded regions conductive. The electrode gap is chosen such that there is no voltage breakdown of EA pads under 5 kV. Copper tapes are used to connect the electrodes with electric wires. Finally, a 0.12 mm thick biaxially-oriented polypropylene (BOPP) tape is used to cover the electrodes formed using the pencil lead. The resulting EA pad is about 0.3 mm thick and weighs 2 g. One EA pad is attached on the outer side of each panel using glue.

V. Experimental Characterisation

A. Torque of the flexural hinge

The flexural hinges connecting the panels of the robot provide the restoring force that allows the skeleton to recover its hexagonal shape when the actuation pressures are removed during the control sequence. The flexural hinges act as torsional springs and their stiffness affects both the forces required to be generated by the pneumatic actuators as well as the restoring forces to recover the initial configuration. We measure the torque vs angular deformation characteristics of the flexural hinge using the Instron 3342 dynamometer as shown in Fig. 6. The flexural hinges both open and close during the robot's movement cycle. We first measure the torque required to open the flexural hinge from 120° to 160°. The torque T_1 representing the torque during the change of angle α from 120° to 160° is given as:

$$T_1 = F_N \cdot l_1 = F \cdot \sin\left(\alpha - \frac{\pi}{2}\right) \cdot l_1 \qquad (7)$$

where the force applied by the bearing on the panel is F_N, the force measured by the load cell is F and l_1 is the distance from the indenter to the hinge. The torque during change of

angle α from 120° to 60° is given as,

$$T_2 = F_N \cdot l_2 = F \cdot \cos\left(\alpha - \frac{\pi}{2}\right) \cdot l_2 \tag{8}$$

where l_2 is the distance from the indenter to the hinge. When the hinge opens from 120° to 160°, the torque increased with the angle, and the maximum torque was 0.019 Nm (Fig. 6(a)). When the hinge compresses to 60°, the required torque increased as the angle decreased, and the maximum torque value was 0.014 N·m (Fig. 6(b)). The average torsional stiffness of the hinge is approximated as $3.27x10^{-4}$ Nm/deg.

B. Bending of the flexural hinge with pneumatic actuator

The pneumatic pouch actuators act as the muscles of the robot and generate the forces to deform the skeleton structure. Firstly, we measured the tension generated by the pouch actuator at different pressures and calculated the torque it applies on the hinge based on geometry. An air compressor is connected to an SMC ITV-212BL4 proportional valve whose output pressure is controlled using an Arduino microcontroller. The maximum torque that can be generated by the pouch actuator is over 0.07 N·m, as shown in Fig. 7, and it far exceeds the maximum restoring torque of the hinge shown in Fig. 6. Thus, the pouch actuator is capable of driving the hinge rotation under a pressure of 100 kPa. We test the pressure versus angular deformation characteristics of a single flexural hinge with pneumatic pouch actuator embedded across it. As Fig. 7(b) shows, applying different air pressures to the pouch actuator controls the angle of the flexural hinge. At zero pressure, the angle between the panels is 120°. At a pressure of 103.1 kPa, the maximum rotation angle of 70° was achieved with approximately 41.7% change.

C. Adhesion force of the electroadhesion actuator

The EA pads need to generate sufficient adhesion force to affix the robot firmly to the ground during the pneumatic actuation for horizontal movement and be able to support the entire weight of the robot during vertical wall-climbing. The electroadhesion force varies from surface to surface and is dependent on properties such as the polarizability and surface roughness. We test the normal and shear adhesion force of the EA pad with three different surfaces over a range of voltages. The EA pad has the best adhesion forces both in normal and shear directions when tested on the phenolic resin board (Fig. 8). At 4.8 kV, the normal adhesion force

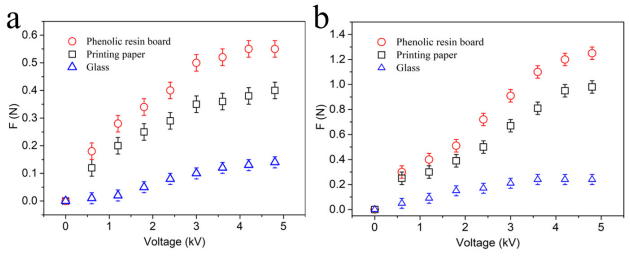

Fig. 8. (a) The measurement of normal force. (b) The measurement of shear force.

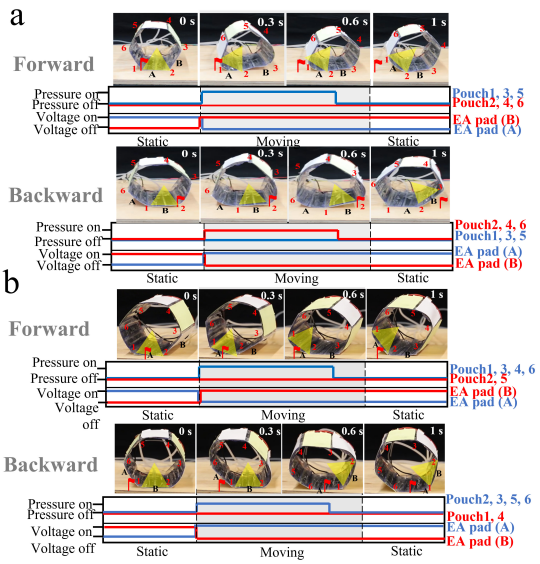

Fig. 9. The two robot's control sequences of rolling on the horizontal surface. (a) The triangle locomotion gait. (b) The rectangle locomotion gait.

is about 0.55 N and the shear adhesion force is about 1.25 N. As the total weight of the robot is 25 g, a single EA pad ensures that the robot adheres to a vertical wall or even hangs from a ceiling. From the forces measured on other materials, we hypothesize that the robot can also traverse vertically on paper but will only be able to traverse horizontally on glass.

VI. Evaluation of Rolling Locomotion

In this section, we discuss the locomotion capabilities of the fully assembled robot in two different preprogrammed gaits - triangle gait and rectangle gait. In the triangle gait, the six pneumatic pouch actuators are connected to two pneumatic inputs (three per input). Similarly, alternate electroadhesion pads are also connected in series forming two sets of electroadhesion actuators. With these connections, the robot is able to execute forward and backward motions by using a simple control sequence without needing prior knowledge of the current position and orientation of the robot. In the rectangle gait, we need to control each pneumatic actuator and EA pad independently but this mode allows the robot to climb steeper inclines.

A. Rolling on the horizontal surface

On a horizontal surface, the robot can rolls forward or backward under the action of the pouch actuators with the help of the EA pads. The process of moving forward and backward in the triangle locomotion gait is detailed in Fig. 9(a) and in the supplementary video. Initially (at time, t=0s), the robot is stationary, all the pouch actuators are at zero pressure and high voltage is applied to the set of EA pads (consisting of the pad labelled A) to affix the robot in its position. The small red flag in the image represents a fixed reference point on the ground. Next, we pressurize pouch actuators 1, 3, and 5 at 100 kPa to rotate the respective

hinges to 70° hinge angle while simultaneously turning off the voltage to the EA pad A. The robot deforms under the action of the pouches and without the constraints of EA pad A, the robot rotates. At the same time, EA pad B is powered by the voltage amplifier. Once EA pad B touches the ground, the pressures in the pouch actuators 1, 3, and 5 are reset to zero making the robot recover its hexagonal shape while the EA pad B firmly attaches to the ground. This full control sequence completes one step of the forward rolling of the robot. To move backward, we change the control sequence of the pouches and the EA pads. First, the pouches 2, 4, and 6 are inflated, and the voltage to EA pad B is set to zero while a high voltage is applied to EA pad A. The robot starts to rotate backwards. Once EA pad A attaches to the ground, we stop actuating the pouches and the robot returns to its equilibrium state.

For the rectangle locomotion gait, we first pressurize pouch actuators 1, 3, 4, and 6 at 80 kPa to rotate the hinges to 90° according to fig. 7(b) while simultaneously turning off the voltage to the EA pad A. The robot begins to deform under the action of the pouches and without the constraints of EA pad A, the robot rotates. At the same time, EA pad B is powered by the voltage amplifier. Once EA pad B touches the ground, the pressures in the pouch actuators 1, 3, 4, and 6 are reset to zero making the robot recover hexagonal shape and EA pad B firmly attaches to the ground. This full control sequence completes one step of the forward rolling of the robot. For backward movement, as Fig. 9(b) shows, we change the control sequence of the pouches and the EA pads. First, the pouches 2, 3, 5, and 6 are inflated, and the voltage to EA pad B is set to zero while a high voltage is applied to EA pad A. The robot starts to rotate backwards. Once EA pad A attaches to the ground, we stop actuating the pouches (2, 3, 5, and 6), and wait for the robot to return to its equilibrium position.

The moving speed of the two locomotion gaits on horizontal surface is about 0.04 m/s or 0.5 BL/s (body-lengths per second) . In addition, with the help of EA pads, the robot displays precise movement. The robot has a displacement error of just 1% in one roll back and forth, in both triangular and rectangular strategies. The percentage error is obtained by comparing the deviation of the displacement with the length of the robot.

B. Climbing an inclined surface

We then test the robot on an inclined surface with different angles, and achieve the maximum traversable angles of 15° and 30° for the triangle and rectangle locomotion gaits respectively (Fig. 10 (a-b)). As we program the control sequence for the forward movement of the robot, the robot successfully climbed up the slope with a speed of 0.027 m/s (0.34 BL/s). We also note that the robot is sometimes able to exhibit horizontal motion even with the EA pads powered off due to the inertia of motion but is unable to climb the inclined plane without utilizing the controllable electroadhesion. This shows the unique advantage of utilising EA pads as feet of the robot and offers promise for rolling locomotion over different terrains.

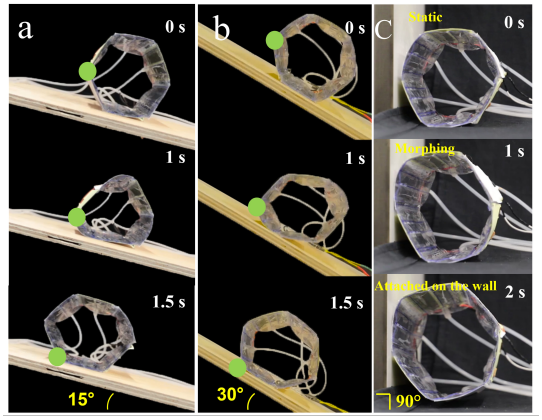

Fig. 10. Sequence of images showing the rolling motion of the robot at inclined surfaces with the maximum angles. (a) The triangle locomotion gait. (b) The rectangle locomotion gait. (c) The robot transitions from a horizontal surface to a vertical wall.

C. Transition from horizontal to vertical surface

Finally, we test the capability of the robot to transition from a horizontal to vertical surface and stay affixed to it with the help of the EA pad. As shown in Fig. 10(c), when the robot is close to the vertical wall, the pneumatic actuators are actuated to position the leading panel closer to the wall. At this moment, the bottom EA pad is turned off and the EA pad on the panel closest to the wall is turned on. This generates electrostatic force that attracts the full panel to the wall and the robot effectively transitions onto the vertical wall. This capability can greatly enhance the practical application of the rolling robot.

VII. Discussion

By comparing with similar rolling robots in recent years, it can be found that the robot in this paper has unique advantages in the following aspects, as shown in Table I.

TABLE I
COMPARISON OF THIS WORK WITH SIMILAR ROLLING ROBOTS

Robots	Speed	Angle	Weight
DEA robot[9]	0.73 BL/s	N/A	0.023 g/cm³
Triangular closed-chain robot[5]	0.1 BL/s	8°	0.052 g/cm³
Shape changing robot [8]	0.23 BL/s	15°	3 g/cm³
This work	0.5 BL/s	30°	0.043 g/cm³

The high moving speed is one of unique advantages of rolling robots. Among the four similar robots, it can be seen that the DEA robot has the fastest moving speed of 0.73 BL/s[9] followed by the robot in this work with a speed of 0.5 BL/s. However, the DEA robot cannot climb inclines due to the lack of adhesion feet, and its motion accuracy is limited due to possibility of slipping. Among the four rolling robots in comparison, the climbing angle of this study is the largest, 30°. In terms of robot mass (density), the robot in this study is relatively lightweight, with a density of about

0.043 g/cm³. In addition, the biggest advantage of this robot is its accuracy in the back-and-forth rolling, with only 0.5% positioning error in a full 360° rolling cycle.

VIII. Conclusions

This paper presents a novel approach towards developing a rolling soft robot using shape-morphing. The robot design integrates distributed soft pneumatic actuators and electroadhesion feet. The pneumatic actuators act as muscles to deform the skeleton of the robot and the EA pads help the robot adhere to surfaces. Utilising these, the robot is able to achieve accurate locomotion on both horizontal and inclined surfaces and also transition from horizontal to vertical surface showcasing the future potential for all-terrain soft robots. With distributed actuation across the robot body, we proposed a simple sequential control strategy that can realize the forward and backward movement of the robot. Robots with versatile locomotion capabilities have potential applications such as remote sensor delivery in dynamic and extreme environments. In future work, we will utilise modelling to optimize the design of the robot and actuators to carry payloads towards realizing untethered capability. Multiple rolling segments for achieving steering capabilities and locomotion on complicated terrains such as vertical walls and ceilings will be investigated. We will also explore the ability of the robot to utilize its shape-morphing capabilities to adapt to changing environments and access cluttered spaces.

References

[1] J. Brackenbury, "Caterpillar kinematics," *Nature*, vol. 390, no. 6659, pp. 453–453, 1997.

[2] R. H. Armour and J. F. Vincent, "Rolling in nature and robotics: A review," *Journal of Bionic Engineering*, vol. 3, no. 4, pp. 195–208, 2006.

[3] Y. Matsumoto, H. Nakanishi, and S. Hirai, "Rolling locomotion of a deformable soft robot with built-in power source," in *Advances In Mobile Robotics*. World Scientific, 2008, pp. 365–372.

[4] N. A. Mansour, T. Jang, H. Baek, B. Shin, B. Ryu, and Y. Kim, "Compliant closed-chain rolling robot using modular unidirectional sma actuators," *Sensors and Actuators A: Physical*, vol. 310, p. 112024, 2020.

[5] J. Wang, Y. Fei, and Z. Liu, "Locomotion modeling of a triangular closed-chain soft rolling robot," *Mechatronics*, vol. 57, pp. 150–163, 2019.

[6] K. Kim, A. K. Agogino, and A. M. Agogino, "Rolling locomotion of cable-driven soft spherical tensegrity robots," *Soft robotics*, vol. 7, no. 3, pp. 346–361, 2020.

[7] J. Wang, D. Gao, and P. S. Lee, "Recent progress in artificial muscles for interactive soft robotics," *Advanced Materials*, vol. 33, no. 19, p. 2003088, 2021.

[8] D. S. Shah, J. P. Powers, L. G. Tilton, S. Kriegman, J. Bongard, and R. Kramer-Bottiglio, "A soft robot that adapts to environments through shape change," *Nature Machine Intelligence*, vol. 3, no. 1, pp. 51–59, 2021.

[9] W.-B. Li, W.-M. Zhang, H.-X. Zou, Z.-K. Peng, and G. Meng, "A fast rolling soft robot driven by dielectric elastomer," *IEEE/ASME Transactions on Mechatronics*, vol. 23, no. 4, pp. 1630–1640, 2018.

[10] D. Rus and M. T. Tolley, "Design, fabrication and control of soft robots," *Nature*, vol. 521, no. 7553, p. 467, 2015.

[11] K. Zhang, C. Qiu, and J. S. Dai, "An extensible continuum robot with integrated origami parallel modules," *Journal of Mechanisms and Robotics*, vol. 8, no. 3, p. 031010, 2016.

[12] S. Li, D. M. Vogt, D. Rus, and R. J. Wood, "Fluid-driven origami-inspired artificial muscles," *Proceedings of the National Academy of Sciences*, vol. 114, no. 50, pp. 13 132–13 137, 2017.

[13] M. A. Robertson, O. C. Kara, and J. Paik, "Soft pneumatic actuator-driven origami-inspired modular robotic "pneumagami"," *The International Journal of Robotics Research*, vol. 40, no. 1, pp. 72–85, 2021.

[14] K. Zhang, Y. Zhu, C. Lou, P. Zheng, and M. Kovač, "A design and fabrication approach for pneumatic soft robotic arms using 3d printed origami skeletons," in *2019 2nd IEEE International Conference on Soft Robotics (RoboSoft)*. IEEE, 2019, pp. 821–827.

[15] H. Kim, Y. Han, D.-y. Lee, J.-I. Ha, and K.-J. Cho, "Sensorless displacement estimation of a shape memory alloy coil spring actuator using inductance," *Smart Materials and Structures*, vol. 22, no. 2, p. 025001, 2012.

[16] M. Salerno, K. Zhang, A. Menciassi, and J. S. Dai, "A novel 4-dof origami grasper with an sma-actuation system for minimally invasive surgery," *IEEE Transactions on Robotics*, vol. 32, no. 3, pp. 484–498, 2016.

[17] A. Chortos, E. Hajiesmaili, J. Morales, D. R. Clarke, and J. A. Lewis, "3d printing of interdigitated dielectric elastomer actuators," *Advanced Functional Materials*, vol. 30, no. 1, p. 1907375, 2020.

[18] J. Cao, L. Qin, J. Liu, Q. Ren, C. C. Foo, H. Wang, H. P. Lee, and J. Zhu, "Untethered soft robot capable of stable locomotion using soft electrostatic actuators," *Extreme Mechanics Letters*, vol. 21, pp. 9–16, 2018.

[19] T. Xu, J. Zhang, M. Salehizadeh, O. Onaizah, and E. Diller, "Millimeter-scale flexible robots with programmable three-dimensional magnetization and motions," *Science Robotics*, vol. 4, no. 29, p. eaav4494, 2019.

[20] A. Li, H. Li, Z. Li, Z. Zhao, K. Li, M. Li, and Y. Song, "Programmable droplet manipulation by a magnetic-actuated robot," *Science advances*, vol. 6, no. 7, p. eaay5808, 2020.

[21] C.-P. Chou and B. Hannaford, "Measurement and modeling of mck-ibben pneumatic artificial muscles," *IEEE Transactions on robotics and automation*, vol. 12, no. 1, pp. 90–102, 1996.

[22] L. Paez, G. Agarwal, and J. Paik, "Design and analysis of a soft pneumatic actuator with origami shell reinforcement," *Soft Robotics*, vol. 3, no. 3, pp. 109–119, 2016.

[23] M. T. Tolley, R. F. Shepherd, B. Mosadegh, K. C. Galloway, M. Wehner, M. Karpelson, R. J. Wood, and G. M. Whitesides, "A resilient, untethered soft robot," *Soft robotics*, vol. 1, no. 3, pp. 213–223, 2014.

[24] O. D. Yirmibeşoğlu, T. Oshiro, G. Olson, C. Palmer, and Y. Mengüç, "Evaluation of 3d printed soft robots in radiation environments and comparison with molded counterparts," *Frontiers in Robotics and AI*, vol. 6, p. 40, 2019.

[25] S. Chen, Y. Cao, M. Sarparast, H. Yuan, L. Dong, X. Tan, and C. Cao, "Soft crawling robots: design, actuation, and locomotion," *Advanced Materials Technologies*, vol. 5, no. 2, p. 1900837, 2020.

[26] Z. Xie, A. G. Domel, N. An, C. Green, Z. Gong, T. Wang, E. M. Knubben, J. C. Weaver, K. Bertoldi, and L. Wen, "Octopus arm-inspired tapered soft actuators with suckers for improved grasping," *Soft robotics*, vol. 7, no. 5, pp. 639–648, 2020.

[27] N. Sholl, A. Moss, W. M. Kier, and K. Mohseni, "A soft end effector inspired by cephalopod suckers and augmented by a dielectric elastomer actuator," *Soft robotics*, vol. 6, no. 3, pp. 356–367, 2019.

[28] J. Shintake, S. Rosset, B. Schubert, D. Floreano, and H. Shea, "Versatile soft grippers with intrinsic electroadhesion based on multi-functional polymer actuators," *Advanced Materials*, vol. 28, no. 2, pp. 231–238, 2016.

[29] M. Graule, P. Chirarattananon, S. Fuller, N. Jafferis, K. Ma, M. Spenko, R. Kornbluh, and R. Wood, "Perching and takeoff of a robotic insect on overhangs using switchable electrostatic adhesion," *Science*, vol. 352, no. 6288, pp. 978–982, 2016.

[30] J. Guo, J. Leng, and J. Rossiter, "Electroadhesion technologies for robotics: A comprehensive review," *IEEE Transactions on Robotics*, vol. 36, no. 2, pp. 313–327, 2019.

[31] S. D. de Rivaz, B. Goldberg, N. Doshi, K. Jayaram, J. Zhou, and R. J. Wood, "Inverted and vertical climbing of a quadrupedal microrobot using electroadhesion," *Science Robotics*, vol. 3, no. 25, p. eaau3038, 2018.

[32] G. Hwang, J. Park, D. S. D. Cortes, K. Hyeon, and K.-U. Kyung, "Electroadhesion based high-payload soft gripper with mechanically strengthened structure," *IEEE Transactions on Industrial Electronics*, vol. 69, no. 1, pp. 642–651, 2022.

[33] R. Niiyama, D. Rus, and S. Kim, "Pouch motors: Printable/inflatable soft actuators for robotics," in *2014 IEEE International Conference on Robotics and Automation (ICRA)*. IEEE, 2014, pp. 6332–6337.